Mechanofluidic Instability-Driven Wearable Textile Vibrotactor

Nathaniel Fino, *Student Member, IEEE,* Barclay Jumet, *Student Member, IEEE,*
Zane A. Zook, *Student Member, IEEE,* Daniel J. Preston, *Member, IEEE*, Marcia K. O'Malley, *Fellow, IEEE*

Abstract— Vibration is a widely used mode of haptic commu-
nication, as vibrotactile cues provide salient haptic notifications
to users and are easily integrated into wearable or handheld
devices. Fluidic textile-based devices offer an appealing plat-
form for the incorporation of vibrotactile haptic feedback, as
they can be integrated into clothing and other conforming and
compliant wearables. Fluidically driven vibrotactile feedback
has primarily relied on valves to regulate actuating frequencies
in wearable devices. The mechanical bandwidth of such valves
limits the range of frequencies that can be achieved, particularly
in attempting to reach the higher frequencies realized with
electromechanical vibration actuators (> 100 Hz). In this paper,
we introduce a soft vibrotactile wearable device, constructed en-
tirely of textiles and capable of rendering vibration frequencies
between 183 and 233 Hz with amplitudes ranging from 23 to
114 g. We describe our methods of design and fabrication and
the mechanism of vibration, which is realized by controlling
inlet pressure and harnessing a mechanofluidic instability. Our
design allows for controllable vibrotactile feedback that is
comparable in frequency and greater in amplitude relative to
state-of-the-art electromechanical actuators while offering the
compliance and conformity of fully soft wearable devices.

I. INTRODUCTION

One of the most important and ubiquitous modes of haptic
feedback is vibration. Vibration has been used to enhance
user experiences across a wide range of applications [1].
Haptic vibrations are commonly delivered to users via small
actuators known as vibrotactors, available in a variety of
forms, including actuators with an eccentric rotating mass
(ERMs), linear resonant actuators (LRAs), voice coil actu-
ators, and piezoelectric actuators. Arrays of these low-cost
actuators can be combined into wearable devices (see, for
example, [2]–[5]) to stimulate the mechanoreceptors in the
skin that respond most actively to vibration [6]. Despite their
widespread adoption, one of the primary drawbacks of these
electromechanical actuators is that they are comprised of
rigid components, which reduce the conformity and wear-
ability of the systems in which they are embedded.

Soft textile-based wearables are an alternative to rigid
electromechanical systems. They can be fully compliant, be
washed, and enable direct integration into clothing [7]. State-
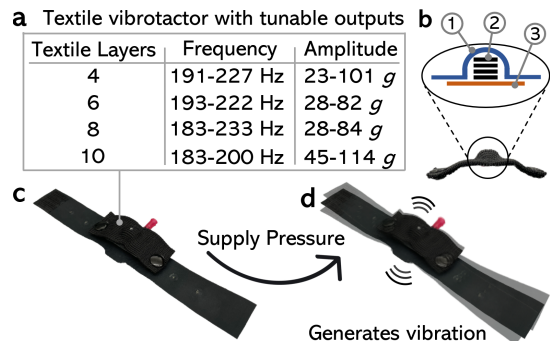of-the-art soft devices often rely on rigid solenoid valves to

Fig. 1. The textile vibrotactor and its operation. (a) Vibration is controlled
by varying inlet pressure and tuned using compliant textile-based snap-on
masses. Each mass comprises three parts: (b1) A top elastic hook-and-loop
strap to fasten to the textile band, (b2) 4 to 10 layers of textiles that serve
to increase the total weight, altering the characteristics of the device, and
(b3) an inelastic hook-and-loop piece to secure the masses to the underside
of the elastic portion. (c) When unpressurized, the device is compliant and
passive. (d) When pressurized, the mechanism generates vibrations.

drive actuation and vibration [8]–[11]. The inclusion of rigid
valves limits the frequency of vibration that can be generated
because their pneumatic actuation must rely on opening
and closing valves to gate pressure, which is inherently
bandwidth-limited. Others have integrated fluidic logic and
soft valves to reduce the physical encumbrance of otherwise
rigid components [12]–[15]. Fluidic control schemes, how-
ever, remain coarser and operate at lower frequencies ($<$
50 Hz) compared to their electronic counterpart systems.
Designing a device capable of high-frequency actuation
within the ideal perceptual range for humans (200–250 Hz)
[16] represents a vital next step in research.

High-frequency vibration without the use of valves to drive
actuation has been demonstrated in soft devices through the
use of silicone or similar elastomers, such as in elastomeric
reed-based vibrotactors [17] and dielectric elastomeric ac-
tuators (DEAs) [18]. Building on this pre-existing research,
we previously developed a hybrid device composed of both
textile and elastomer components, which was capable of
producing vibrations that range between 160 and 260 Hz
at 13 to 38 g, through a single pressure input of 0.3 to
1.4 bar [19]. This elastomer-based vibrotactile feedback
device operates on the principle of mechanical hysteresis
(i.e., a system state–dependent behavior), where vibration
occurs due to a mechanical bias that is acted against by
the inflation—and causal pressurization—of the device. This
fluid-induced mechanical hysteresis drives high-frequency
vibration, free of tethered solenoids. Using the principles of

self-actuation through mechanical hysteresis, we investigate the possibility of achieving similar characteristics using only textiles. **Through this prototype textile design, we test the most fundamental components of this new actuation strategy with a focus on achieving high frequency and amplitude vibrations with a device fabricated solely with textile materials. Additionally, a fully textile structure introduces attractive improvements such as reduced manufacturing complexity and cost and achieves this with a form factor that enables more seamless integration into garments and other textile-based systems.**

In this work, we introduce a soft wearable vibrotactor made completely of heat-sealable textiles (HSTs) and hook-and-loop fasteners (Fig. 1) **that does not rely on typical commercially available electromechanical motors to achieve vibration**. We demonstrate the tunability of this device in terms of its output frequency and peak-to-peak force amplitudes, realized by interchanging modular masses to produce vibrotactile frequencies in the range of 183 to 233 Hz and amplitudes of 23 to 114 g. We present the design, fabrication, and experimental validation of our device, which achieves oscillatory actuation through harnessing inherent mechanical hysteresis and fluidic instabilities. We further demonstrate the performance of this device and establish its validity against our previous work [19] **that relied on a combination of textile and elastomeric materials to achieve vibration**, other soft wearable fluidic devices, and commercially available electromechanically actuated alternatives. **Our device enables us to realize vibrations in a larger range of amplitudes and at comparable frequencies to those of commercially available LRAs and ERMs and is presented in a fully compliant and wearable form factor. The shift to a fully textile architecture allows us to achieve vibration in a device that is smaller in size, lower in profile, one-third the weight, four times faster to fabricate, and lower in cost compared to our prior design that used elastomeric materials.**

II. DEVICE DESIGN AND OPERATION

When designing soft wearable devices, textiles are an appealing material choice due to their ubiquity in wearables, their inherent compliance, and the simple, scalable methods of fabrication to which they are suited [20], [21]. Furthermore, textile materials, particularly heat sealable textiles (HSTs) and hook-and-loop fasteners, are low-cost and easy to employ, and they can be fabricated at home using simple tools, such as a vinyl cutter and household iron. Given these appealing features, we developed a vibrotactile wearable device comprised entirely of textile-based components. In the following sections, we describe the design, materials, and fabrication methods that we used to realize our device.

We designed and sized our vibrotactor to be worn on the wrist, given that the wrist is a common location for wearable devices like smartwatches and fitness trackers. A textile band, comprised of HSTs, serves as the foundation of the vibrotactor, providing an attachment point for the interchangeable masses that govern the vibrotactile characteristics of the
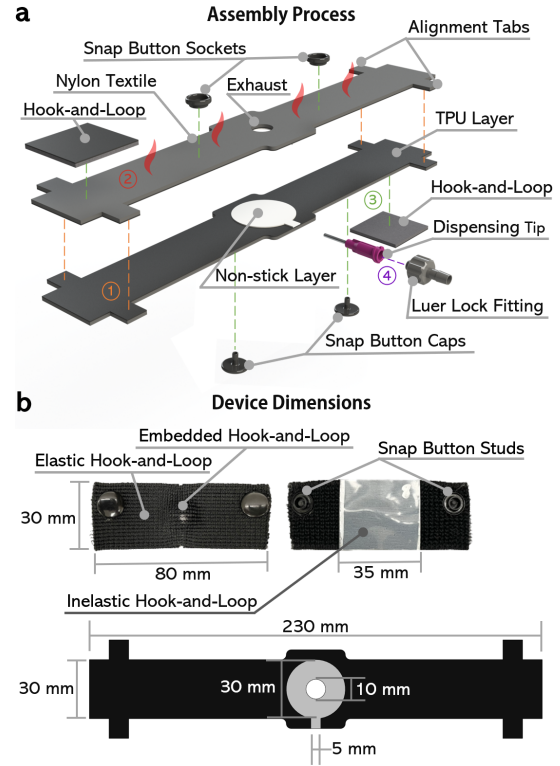

Fig. 2. Overview of design. (a) Assembly process: (1) alignment tabs orient the two halves of cut textile for heat pressing; (2) heat pressing thermally bonds the HSTs at 195° C with an applied pressure of 3.45 bar for 25 s; (3) hook-and-loop fasteners and snap buttons are attached; (4) Luer lock dispensing tip inserted into band and secured using epoxy for a quick-connect pneumatic input. (b) The modular textile mass used in the textile vibrotactor is comprised of 4, 6, 8, or 10 layers of 10-mm by 10-mm hook-and-loop layers and is embedded between the attached elastic and inelastic hook-and-loop textiles.

device. The interchangeable assembly of masses includes an elastic hook-and-loop strap and an inelastic hook-and-loop base that fastens the embedded hook-and-loop layers to the elastic strap. Lastly, snap buttons are added to aid in quickly adding or removing the interchangeable masses to the textile band, as shown in Fig. 2.

The vibrotactor is manufactured using 2D manufacturing processes such as vinyl cutting (Maker 3, Cricut) and heat pressing (DK20SP, Digital Knight) for fabrication, similar to the steps described in our prior work [19]. We initialize the process by cutting out a square of HST (FHST, Seattle Fabrics) and placing it on the vinyl cutter. Once loaded, the vinyl cutting machine cuts the exterior shape of the band, including an intermediate layer, adhesive-backed paper (DL8511FS, Packzon), to prevent thermal bonding in predetermined regions so as to allow fluidic transport, as shown in Fig. 2a. **Once the textile has been cut, the adhesive mat is removed from the vinyl cutting machine and the extraneous paper and textile is discarded.** The two halves of the textile band are aligned using the alignment tabs and heat pressed. Once heat-pressed, the textile band is cold-pressed to ensure stronger adhesion. After pressing the device, the adhesive-backed hook-and-loop fasteners
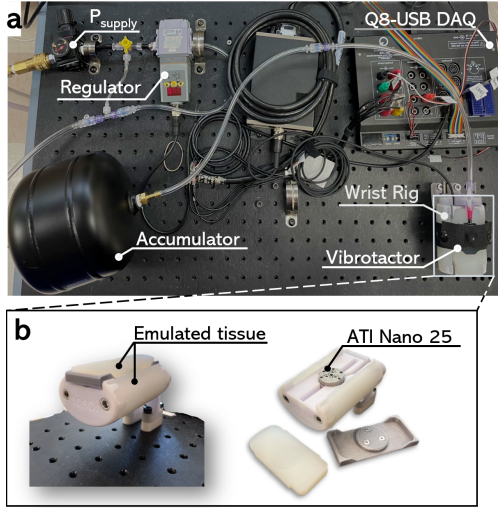
Fig. 3. Experimental testbed. (a) The hardware is laid out on a mechanical breadboard, comprising the regulator and accumulator to maintain constant pressure upstream of the vibrotactor and the DAQ to interface with electronics. (b) The wrist rig used for data collection uses an ATI Nano25 load cell providing forces in the X, Y and Z directions. To capture the forces from the textile vibrotactor, the forces in the Z-axis were used.

(94985K35, McMaster-Carr) and snap buttons (KZ, Better-Jonny) are attached to the textile band to fasten the band to the user. Finally, the alignment tabs are cut and the Luer lock dispensing tip (JG13-0.5HPX, Jensen Global), and a quick-turn Luer lock fitting (51525K123, McMaster-Carr) are added. Similarly, the interchangeable masses used to change vibrotactor characteristics are comprised of cut elastic (WRISTBAND, gymboss), inelastic hook-and-loop fasteners (94985K35, McMaster-Carr), and plastic snap buttons (KZ, BetterJonny) as shown in Fig. 2a,b.

Our textile vibrotactor operates on the principle of mechanical hysteresis [22], delineated into distinct states based on the competing interactions between the textile masses and pressures: unpressurized (1,6) ($P_{in} = 0$), under-pressurized (2) ($P_{in} < 0.2$ bar) as the device actuates at pressures beyond 0.2 bar, sealed valve (3,5) ($\Delta P <$ Breakthrough) and open valve ($\Delta P \geq$ Breakthrough) (4) as shown in Fig. 4a. The process of repeating states 3–5 generates the oscillatory vibration and is discussed more deeply in our previous work [19].

III. DEVICE CHARACTERIZATION

We explore the effect that varying textile masses and pressures have on vibration frequency, vibration amplitude, flow rate, and power consumption. We also test the dampening caused by various clothing materials to simulate the salience of cues in real-world applications. To conduct these experiments, we used a test rig (Fig. 3b) where the band was fastened with one of the four interchangeable masses and varied the input pressure from 0.1 to 1.5 bar.

A. Textile vibrotactor characterization

We supplied a high-pressure source, a compressed air line into an electropneumatic regulator (8083T1, McMaster-Carr), regulating pressure from 0.1 bar to 1.5 bar in 0.1-bar increments. An accumulator (NY-16, NYAIR) was connected downstream to the pressure regulator, acting as a pneumatic capacitor for the system. An ATI Nano25 load cell embedded in the wrist rig measured the forces generated by the vibrotactor. Before each trial, we fastened the textile vibrotactor to the wrist rig with a 2-N preload. **The shape of the rig allows the band to be preloaded as it would be on the user's wrist. This preload is required to ensure a consistent mechanical bias, which is necessary to achieve the vibrotactile effect. The force sensor on the wrist rig was used to characterize the vibrations and to ensure that a consistent preload was applied across all trials.** After zeroing the load cell, an 8-channel data acquisition (DAQ) device (Q8-USB DAQ, Quanser) recorded data for analysis. The raw force data at steady state were filtered using a second-order low-pass Butterworth filter with a cutoff frequency of 400 Hz and a sampling frequency of 1000 Hz. Once filtered, the time-series data were transformed to the frequency domain through a Fast Fourier Transform (FFT). Finally, the data were rearranged using the fftshift command in MATLAB to shift the zero-frequency component to the center of the frequency spectrum to properly scale the frequency values. **Vibration amplitude was determined by analyzing the last 5 s of force data from the 10-second-long experimental trial to ensure that our device reached steady-state operation. The peak-to-peak amplitudes of force were extracted from the data and converted to g by dividing by the force of gravity times the respective device weight. Results are averaged across all cycles that occurred in that 5-s period.**

In a similar manner, we measured the power consumption by supplying a laboratory-fed air source into a manual pressure regulator (PR364, Parker Hannifin) and modulating the pressure from 0.1 bar to 1.5 bar in 0.1-bar increments, verified by a pressure gauge (MG1-30-A-9V-R, SSI Technologies), with the same accumulator as in other tests. A flow meter (FLR1004-D, Omega) between the accumulator and vibrotactor reported the corresponding flow rate. We report the power in Watts, through the conversion of pressure and flow rate, to compare more easily to electronic counterparts.

B. Device comparisons

We compared the performance of our textile-based vibrotactor to published characteristics of performance for other commercially available and valve-based haptic devices. We examined the vibration frequency, vibration amplitude, flow, and power consumption, represented in Table I. Notably, the amplitudes for devices (6) and (7) were calculated using reported forces and weights [8], [9].

C. Cue salience characterization

To collect the range of forces transmitted through clothing, we attached both the textile vibrotactor and a commercially available C-2 tactor to the wrist rig. Both vibrotactors were actuated at their maximum amplitudes (occurring at a frequency of 250 Hz for the C-2 tactor and a pressure of 1.5 bar for the textile vibrotactor). We conducted a parametric sweep
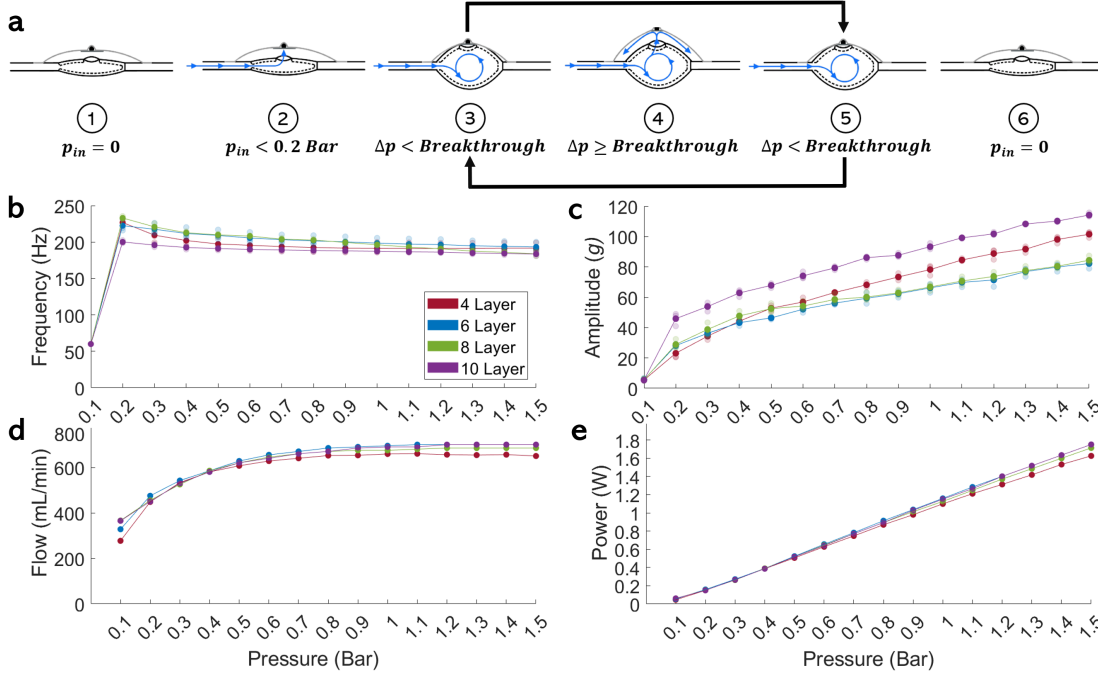
Fig. 4. Actuation stages and vibration output of the textile-based vibrotactor. (a) The textile vibrotactor has distinct states, namely unpressurized (1,6), under-pressurized (2), and vibrating (3-5). (b) The textile vibrotactor has a total frequency range of 183 to 233 Hz (c) The device achieves an amplitude range of 23 to 114 g, based on the attached masses ranging from 4 layers to 10 layers of textile. (d) The flow through the textile vibrotactor for each of the interchangeable masses is varied to evaluate power consumption. (e) Minimum to maximum power consumption of each interchangeable mass for input pressures ranging from 0.1 to 1.5 bar.

for materials, where forces recorded with no intermediate material represented a baseline; the materials included faux leather, a cotton t-shirt, a polyester fabric (Dryfit) shirt, a polyester-cotton-mixed sweater, and microfiber cloth.

IV. RESULTS

A. Textile vibrotactor performance

We compared vibration frequencies and amplitudes as we varied the modular textile masses. We observe higher vibration amplitudes with the 4- and 10-layer masses, and higher vibration frequencies with the 4- and 8-layer masses (Fig. 4b,c). Though there are similarities in the ranges of vibration frequency and amplitude, no individual mass covers the full range of frequencies and amplitudes. The 4-layer mass covers most of the range, but falls short at lower frequencies compared to the 183 Hz exhibited by the 8- and 10-layer masses. The 10-layer mass allows for an extra 13 g. By using modular textile masses, we demonstrate a wider range of possible outputs than that of a single mass. We note that textile masses with two or fewer layers did not consistently exhibit oscillatory behavior due to the diminished mechanical bias with these smaller masses.

We also examined the dependence of flow rate on pressure, presented in Fig. 4d. Most notably, we observe a plateau of the flow rate around 0.8 bar, agreeing with the asymptotic behavior of frequency at approximately 0.8 bar in Fig. 4b. The power consumption is linearly correlated with pressure, ranging from a minimum average of 0.057 watts to a maximum average of 1.710 watts, as shown in Fig. 4e, yet power

has no obvious correlation with different textile masses.

B. Device comparisons

We compare vibration frequency and amplitude of our textile vibrotactor to valve-based soft devices reported in the literature **and to published specifications of commercially available vibrotactors (Table I)**. As expected, we find the achievable frequencies of the valve-based devices are limited by electromechanical valves to a maximum of 7 Hz for devices (6, 10) and 50 Hz for device (7), orders of magnitude less than the 233 Hz reported here for our textile vibrotactor. Additionally, the maximum peak-to-peak amplitudes are 14.82 and 6.27 g for devices (6,7), respectively, compared to the 114 g of the textile vibrotactor.

Comparing frequency, amplitude, and power, the TacHammer produces a maximum frequency of 155 or 200 Hz and an amplitude of 15.5 or 27 g, depending on the mode (traditional or impact), all of which are less than the 300 Hz and 33 g of the C-2 tactor and the 233 Hz and 114 g of the textile vibrotactor. **Our fluidically-driven vibrotactile device has lower maximum power requirements than the commercially available C-2 tactor but requires more power in the standard operating range than the TacHammer.** The operating power (the power consumption at the ideal operating regime) of the TacHammer was 26.1 or 20.6 mW, based on the mode, compared to the 375 mW of the C-2 tactor and 867 to 914 mW of the textile vibrotactor (dependent on mass). Although only one device—the C-2 tactor—reported the maximum power, our textile device has a 22–28% lower maximum power consumption.

TABLE I
COMPARISON OF VIBRATION FREQUENCIES AND AMPLITUDES FOR ACTUATORS AND DEVICES

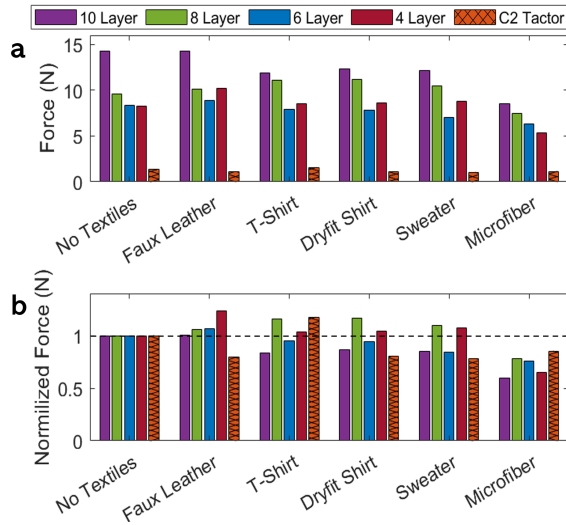| Tactors/Devices		Min Frequency (Hz)	Max Frequency (Hz)	Min Amplitude (g)	Max Amplitude (g)	Frequency Range (Hz)	Amplitude Range (g)	Weight (g)	Max Power (mW)	Operating Power (mW)	Cost (Dollars)
Textile-Based Vibrotactors											
(1)	4 Layer	191	227	23	101	36	78	8.97	1630	867	2.22
(2)	6 Layer	193	222	28	82	29	54	8.98	1750	914	2.23
(3)	8 Layer	183	233	28	84	50	56	9.07	1710	894	2.25
(4)	10 Layer	183	200	45	114	17	69	9.11	1750	894	2.27
(5)	Hybrid [19]	160	260	13	38	100	25	30	-	-	3.19
Valve-Based Soft Devices											
(6)	Bellowband [8]	0	7	0	14.82	7	14.82	11	-	-	-
(7)	PneuSleeve [9]	0	50	0	6.27	50	6.27	26	-	-	-
(8)	PneuMod [10]	0	7	-	-	7	-	-	-	-	-
Commercial Actuators											
(9)	TacHammer (Traditional)	0.5	200	2	15.5	199.5	13.5	15	-	26.1	50
(10)	TacHammer (Impact)	0.5	155	15	27	154.5	12	15	-	20.6	50
(11)	C-2 Tactor	200	300	0	33	100	33	17	2250	375	210

Fig. 5. (a) Comparison of textile vibrotactor and C-2 tactor based on force outputs with no textiles and with an intermediate clothing material: faux leather, 100% cotton t-shirt, 100% polyester fabric (Dryfit) shirt, 50/50 polyester cotton mixed sweater, and a microfiber cloth. (b) Effects of dampening and the consequent attenuation (forces normalized to baseline).

C. Cue Salience

Results presented in Fig. 5a show a downward trend of force compared to the decreases in compliance from faux leather to microfiber, displaying the impact made by more compliant materials attenuating the force output. Results also show that some combinations of interchangeable mass in the vibrotactor and intermediate material result in increased force output, particularly for 4-layer and 8-layer interchangeable masses with faux leather, t-shirt, dryfit shirt, and sweater (see Fig. 5b). This behavior is also observed for the C-2 tactor, but only in its interaction with the t-shirt material.

V. DISCUSSION

A. Comparing soft vibrotactors

We experimentally compared the performance of our fully textile vibrotactor against that of the hybrid vibrotactor introduced in our previous work [19], (Table I, device (5)). We present the range of frequencies and amplitudes achievable with each vibrotactor and the device weight. The range of amplitudes for the textile vibrotactor is three times greater than that of the hybrid vibrotactor, despite being a third of the weight, yet the frequency range is narrower, despite the additional masses used to tune the maximum frequency range. With a comparable frequency range and larger amplitude range than our hybrid vibrotactor, we demonstrate the feasibility of using textiles to drive vibrations through mechanofluidic instabilities.

B. Comparing textile wearables and vibrotactile Actuators

Experimentally comparing the performance of our fully textile device against the valve-based devices shown in Table I, we observe a large increase from low-frequency vibrations (0 to 7 Hz in devices (6,8) and 0 to 50 Hz in device (7)) to high-frequency vibrations (183 to 233 Hz). The amplitude ranges produced by the textile vibrotactor greatly exceed what is produced by any of the reported valve-based devices. This ability to convey high frequency and high amplitude demonstrates the benefits of self-actuated vibration driven through fluidic instabilities in a fully textile-based device.

To further validate the design and characteristics of the textile vibrotactor, **we compared its performance to published specifications of two commercially available electromechanical vibrotactors with large dynamic ranges**, namely the C-2 tactor and the TacHammer. We show the comparable ranges of frequency for our textile vibrotactor, between the range of the C-2 tactor and above the range of the TacHammer, while exceeding the amplitude outputs by more than three times the highest-amplitude commercial device. Our textile-based vibrotactile wearable has comparable performance in a form factor that is fully soft, lightweight, and low-cost compared to these commercially available devices.

C. Cue salience through layered clothing

The compliant materials typically used to embed electromechanical vibrotactors absorb and dampen the deliverable force and amplitudes of vibration that are transmitted to the user, reducing cue salience. With our high-amplitude textile-based vibrotactor, we demonstrate that vibrations are successfully transmitted in the presence of an intermediate material. As shown in Fig. 5, despite being affected by the softer materials, the textile vibrotactor was capable of producing forces ranging from 8 to 14 N, four to seven times greater than that of the C-2 tactor. Our device was less susceptible to dampening through clothing layers for four of the five materials shown in Fig. 5b. Moreover, all materials except for the microfiber amplify vibrations generated by the 4- and 6-layer masses. Given that the textile vibrotactor is fully textile, high-amplitude, and low-cost, it is well-suited to integration within garments and larger-scale textile systems without concern for diminished cue salience.

VI. CONCLUSIONS

In this paper, we present a wearable and compliant haptic device—comprised solely of textiles and hook-and-loop material—capable of producing high-frequency vibration without the need for high-frequency switching of solenoid valves. The achievable range of vibration frequencies and amplitudes is tunable through the use of interchangeable masses. Vibrotactile actuation is realized through mechanical hysteresis, which is possible due to a biased state of the device. We demonstrated the dynamic range of the textile vibrotactor by varying the input pressure, resulting in vibrotactile ranges of frequency and amplitude between 183–233 Hz and 23–114 g, respectively. We compared this textile-based vibrotactor to other soft wearable devices in research and commercially available electromechanical tactile feedback devices. We found that our device provides vibrotactile cues in similar frequency ranges but at higher amplitudes than other devices, producing a haptically capable device that is more immune to the effects of intermediate clothing, comparable in **max** power consumption, lower cost, and lighter weight than the state of the art.

REFERENCES

[1] S. Choi and K. J. Kuchenbecker, "Vibrotactile display: Perception, technology, and applications," *Proceedings of the IEEE*, vol. 101, pp. 2093–2104, Sep. 2013.

[2] E. Pezent, P. Agarwal, J. Hartcher-OrBrien, N. Colonnese, and M. K. O'Malley, "Design, control, and psychophysics of tasbi: A force-controlled multimodal haptic bracelet," *IEEE Transactions on Robotics*, vol. 38, no. 5, pp. 2962–2978, 2022.

[3] A. S. Macklin, J. M. Yau, and M. K. O'Malley, "Evaluating the effect of stimulus duration on vibrotactile cue localizability with a tactile sleeve," *IEEE Trans. on Haptics*, vol. 14, no. 2, pp. 328–334, 2021.

[4] C. M. Reed, H. Z. Tan, Z. D. Perez, E. C. Wilson, F. M. Severgnini, J. Jung, J. S. Martinez, Y. Jiao, A. Israr, F. Lau, *et al.*, "A phonemic-based tactile display for speech communication," *IEEE Transactions on Haptics*, vol. 12, no. 1, pp. 2–17, 2018.

[5] S. Choi and K. J. Kuchenbecker, "Vibrotactile display: Perception, technology, and applications," *Proceedings of the IEEE*, vol. 101, no. 9, pp. 2093–2104, 2013.

[6] M. K. O'Malley and A. Gupta, "Haptic interfaces," *HCI beyond the GUI: Design for Haptic, Speech, Olfactory, and other nontraditional Interfaces*, pp. 25–64, 2008.

[7] C. Thalman and P. Artemiadis, "A review of soft wearable robots that provide active assistance: Trends, common actuation methods, fabrication, and applications," *Wearable Technologies*, vol. 1, p. e3, 2020.

[8] E. M. Young, A. H. Memar, P. Agarwal, and N. Colonnese, "Bellowband: A pneumatic wristband for delivering local pressure and vibration," in *2019 IEEE World Haptics Conference*, pp. 55–60.

[9] M. Zhu, A. H. Memar, A. Gupta, M. Samad, P. Agarwal, Y. Visell, S. J. Keller, and N. Colonnese, "PneuSleeve: In-fabric multimodal actuation and sensing in a soft, compact, and expressive haptic sleeve," in *Proceedings of the 2020 CHI Conference on Human Factors in Computing Systems*, pp. 1–12.

[10] B. Zhang and M. Sra, "Pneumod: A modular haptic device with localized pressure and thermal feedback," in *Proceedings of the 27th ACM Symposium on Virtual Reality Software and Technology*, VRST '21, (New York, NY, USA), Association for Computing Machinery, 2021.

[11] M. Zhu, T. N. Do, E. Hawkes, and Y. Visell, "Fluidic fabric muscle sheets for wearable and soft robotics," *Soft robotics*, vol. 7, no. 2, pp. 179–197, 2020.

[12] S. Song, S. Joshi, and J. Paik, "Cmos-inspired complementary fluidic circuits for soft robots," *Advanced Science*, vol. 8, no. 20, p. 2100924, 2021.

[13] D. J. Preston, P. Rothemund, H. J. Jiang, M. P. Nemitz, J. Rawson, Z. Suo, and G. M. Whitesides, "Digital logic for soft devices," *Proceedings of the National Academy of Sciences*, vol. 116, no. 16, pp. 7750–7759, 2019.

[14] C. J. Decker, H. J. Jiang, M. P. Nemitz, S. E. Root, A. Rajappan, J. T. Alvarez, J. Tracz, L. Wille, D. J. Preston, and G. M. Whitesides, "Programmable soft valves for digital and analog control," *Proceedings of the National Academy of Sciences*, vol. 119, no. 40, p. e2205922119, 2022.

[15] A. Rajappan, B. Jumet, R. A. Shveda, C. J. Decker, Z. Liu, T. F. Yap, V. Sanchez, and D. J. Preston, "Logic-enabled textiles," *Proceedings of the National Academy of Sciences*, vol. 119, no. 35, p. e2202118119, 2022.

[16] V. B. Mountcastle, R. H. LaMotte, and G. Carli, "Detection thresholds for stimuli in humans and monkeys: comparison with threshold events in mechanoreceptive afferent nerve fibers innervating the monkey hand.," *Journal of Neurophysiology*, vol. 35, no. 1, pp. 122–136, 1972.

[17] E. Kitamura, H. Nabae, G. Endo, and K. Suzumori, "Self-excitation pneumatic soft actuator inspired by vocal cords," vol. 331, p. 112816.

[18] E. Hajiesmaili and D. R. Clarke, "Dielectric elastomer actuators," *Journal of Applied Physics*, vol. 129, no. 15, p. 151102, 2021.

[19] N. Fino, Z. A. Zook, B. Jumet, M. K. O'Malley, and D. J. Preston, "A soft approach to convey vibrotactile feedback in wearables through mechanical hysteresis," *Robosoft*, 2022.

[20] V. Sanchez, C. J. Walsh, and R. J. Wood, "Textile technology for soft robotic and autonomous garments," *Advanced Functional Materials*, vol. 31, no. 6, p. 2008278, 2021.

[21] B. Jumet, M. D. Bell, V. Sanchez, and D. J. Preston, "A data-driven review of soft robotics," *Advanced Intelligent Systems*, vol. 4, no. 4, p. 2100163, 2022.

[22] L. C. van Laake, J. de Vries, S. Malek Kani, and J. T. Overvelde, "A fluidic relaxation oscillator for reprogrammable sequential actuation in soft robots," *Matter*, vol. 5, no. 9, pp. 2898–2917, 2022.